RSC Advances

PAPER

View Article Online
View Journal | View Issue

Cite this: *RSC Adv.*, 2016, **6**, 111374

Hierarchical ZnO nanorods/$Ni(OH)_2$ nanoflakes for room-temperature, cheap fabrication of non-enzymatic glucose sensors†

V. Strano* and S. Mirabella

Received 2nd September 2016
Accepted 16th November 2016

DOI: 10.1039/c6ra22062b

www.rsc.org/advances

Hierarchical nanostructures composed of $Ni(OH)_2$ nanoflakes on ZnO nanorods (NRs) are fabricated by a low-cost, fully chemical method at room-temperature. The morphological features of the ZnO NRs were varied (by changing the chemical bath deposition parameters) in terms of height and lateral size. ZnO NRs provide a large surface area substrate for the pulsed electrodeposition of nanostructured $Ni(OH)_2$. The correlation between the synthetic parameters, the final structure and the electrochemical behavior of $Ni(OH)_2$/ZnO nanostructures is investigated. The enzyme-free oxidation of glucose at the surface of electrodeposited $Ni(OH)_2$ is demonstrated in 0.1 M NaOH, revealing that a proper choice of the electrodes fabrication conditions improves the glucose sensitivity up to 1.85 mA cm^{-2} mM^{-1}, with a linear detection range of 0.04–2.10 mM. All the samples show a fast response time (less than 1 s), resistance in chloride solution, selectivity in the presence of common interfering electroactive species and excellent long-term stability. All these features, combined with the ease of the fabrication method, make $Ni(OH)_2$/ZnO nanostructures an ideal alternative for inexpensive amperometric glucose sensing applications.

Introduction

Hierarchical nanostructures are the focus of a large part of the recent research in material science. The ability to design nanomaterials composed of multiple components, with different geometries and properties, is opening new opportunities for enhancing material–environment interaction.[1] However, for practical uses, it is needed that the development of high efficiency nanomaterials is accompanied by low-cost and feasible large scale synthesis. This is even more important for the technology underlying the glucose level monitoring, which is a fundamental issue for human health, industrial food and biotechnological applications.[2–4]

Recently, numerous approaches have been proposed for amperometric non-enzymatic glucose sensors, having the advantages of overcoming many of the drawbacks related to conventional enzymatic technology.[2,4,5] The non-enzymatic sensing mechanism exploits the possibility to oxidize the glucose directly on an electrode surface characterized by the presence of electrocatalyst species. A few materials, such as polymers,[3] metals,[6] metal oxides and hydroxides[7] have been shown to be suitable as working electrode in non-enzymatic glucose sensors. Among them, nickel hydroxide [$Ni(OH)_2$] has shown great potential in terms of high-sensitivity, response time and glucose concentration range.[7–9] The electrochemical activity of $Ni(OH)_2$ is due to the transition from Ni^{2+} to Ni^{3+} oxidation state at a given potential leading to the formation of the catalytically active nickel oxyhydroxide (NiOOH) species, which starts the glucose oxidation.[5] Since the latter is a surface process, maximizing the surface area, as well as ensuring an efficient electron transport, can allow to enhance the performance of the $Ni(OH)_2$-based sensor. In addition to the direct synthesis of high surface area Ni-based nanostructures,[10,11] a promising approach is the fabrication of modified electrodes, consisting of nanocomposites or hierarchical nanostructures in which a very thin film of $Ni(OH)_2$, deposited on a nanostructured substrate, acts as the glucose oxidizing element.[2,3,8,9,12–17] In particular, zinc oxide (ZnO) nanostructures have proven to be an excellent substrate for the deposition of $Ni(OH)_2$.[16,18] They provide a number of advantages such as good electrical conductivity, non-toxicity and the possibility to be deposited *via* low-cost methods. Recently, we demonstrated that in the chemical bath deposition of ZnO NRs, the variation of HMTA concentration significantly affects the morphology of ZnO NRs due to the *shape inducing* function played by HMTA that promotes the vertical growth along the [0001] axis.[19,20] Therefore, a fine tuning of the aspect ratio of the nanorods can be easily achieved by varying the HMTA amount in the synthetic solution. Many papers, reporting on hierarchical nanostructures and nanocomposites containing $Ni(OH)_2$ as active material, verified some dependence of the electrochemical

IMM-CNR Matis, Dipartimento di Fisica e Astronomia, Università di Catania, via S. Sofia 64, 95123 Catania, Italy. E-mail: vincenzina.strano@ct.infn.it

† Electronic supplementary information (ESI) available: Additional SEM images, EDX and CV. See DOI: 10.1039/c6ra22062b

properties on the underlying material.[13,18,21] Lo *et al.* have recently demonstrated that in the high-performance supercapacitor electrodes based on ZnO/$Ni(OH)_2$ nanocomposites, the ZnO nanowires, primarily used as support for $Ni(OH)_2$ nanoflakes, also enhanced the electrical conductivity of the electrode.[18]

The aim of this work is to investigate a fully-chemical, simple and cost-effective synthetic method for the fabrication of a glucose sensing electrode employing hierarchical nanostructures with $Ni(OH)_2$ flakes onto ZnO nanorods (NRs). The influence of the nanostructure morphology on the performance of the sensing electrodes is investigated, revealing that sensing properties can be enhanced by just an appropriate choice of the synthetic parameters.

Experimental section

a. Chemical bath deposition of ZnO nanorods arrays

ZnO nanorods (NRs) were grown on commercial indium tin oxide (ITO) substrate (working area 1 cm × 1 cm) by chemical bath deposition (CBD).[19,22,23] The substrates were cleaned in ultrasonic baths of acetone, isopropanol, then rinsed with deionized (DI) water (MilliQ, 18 MΩ cm) and dried with N_2 gas. A seed layer of ZnO crystallites was obtained by spin-coating a 5 mM ethanolic solution of zinc acetate dihydrate $(CH_3COO)_2Zn\cdot 2H_2O$ (Sigma-Aldrich puriss. p. a., ACS reagent, ≥99.0%) at 1000 rpm for 60 seconds, followed by annealing on a hot plate (at 240 °C in air for 20 minutes). Thereafter, the ZnO NRs arrays were grown by vertically immersing the seeded samples in 200 mL DI water solution containing 25 mM zinc nitrate hexahydrate $Zn(NO_3)_2\cdot 6H_2O$ (Sigma-Aldrich purum p. a. crystallized, ≥99.0%) and 25 or 50 mM hexamethylenetetramine $C_6H_{12}N_4$ (HMTA, Sigma-Aldrich puriss. p. a., Reag. Ph. Eur., ≥99.5%) at 90 °C for 1 h. After the growth, the samples were rinsed with DI water and dried with N_2 gas.

b. Electrodeposition of $Ni(OH)_2$

Nanostructured flakes of $Ni(OH)_2$ were deposited onto ZnO NRs by pulsed electrodeposition in an aqueous solution containing 5 mM nickel nitrate hexahydrate $Ni(NO_3)_2\cdot 6H_2O$ (Sigma-Aldrich, 99.999%, trace metals basis) at room temperature. The deposition was carried out using a VersaStat 4 potentiostat in a three electrode cell using ZnO NRs arrays, saturated calomel electrode (SCE) and platinum wire as working, reference and counter electrodes, respectively. The deposition mechanism may be consistent with the following reactions:[18,24]

$$(NO_3)^- + H_2O + 2e^- \rightarrow (NO_2)^- + 2OH^- \quad (1)$$

$$Ni^{2+} + 2OH^- \rightarrow Ni(OH)_2 \quad (2)$$

After nickel nitrate dissociation, the reduction of $(NO_3)^-$ ions occurring at the cathode drives the precipitation of $Ni(OH)_2$ onto NRs. The pulsed electrodeposition was performed with a fixed current density at 1 mA cm^{-2} (1 s as current-on time, 10 s as current-off time), and with deposition cycles in the range 20–60. The samples were then rinsed with DI water and dried in air. The samples are labeled with two numbers, indicating the HMTA molar concentration (for the synthesis of ZnO NRs) and the number of electrodeposition cycles (for the synthesis of $Ni(OH)_2$ flakes).

c. Characterization

The surface morphology of the samples was analyzed by using a FE-SEM (Gemini field emission – scanning electron microscope Carl Zeiss SUPRA 25) combined with energy dispersive X-ray spectroscopy (EDX). All electrochemical characterizations of the samples were performed at room temperature using the VersaStat 4 potentiostat in three electrodes configuration, with 0.1 M NaOH solution as electrolyte (pH 13).

Results and discussion

ZnO NRs with different morphological properties were obtained with 25 and 50 mM HTMA and fixed concentration of zinc nitrate hexahydrate (25 mM). As shown in Fig. 1(a) and (b), the ZnO NRs, with a well-defined hexagonal prism shape, are arranged in a uniform array on ITO substrate. The average values of the lateral size, *d*, and height, *h*, of ZnO NRs were extracted from SEM analyses and reported in the Table 1.

Thereafter, the ZnO NRs grown at different HMTA concentration were uniformly covered with $Ni(OH)_2$ nanoflakes, subjecting the samples to a variable number of cycles of pulsed

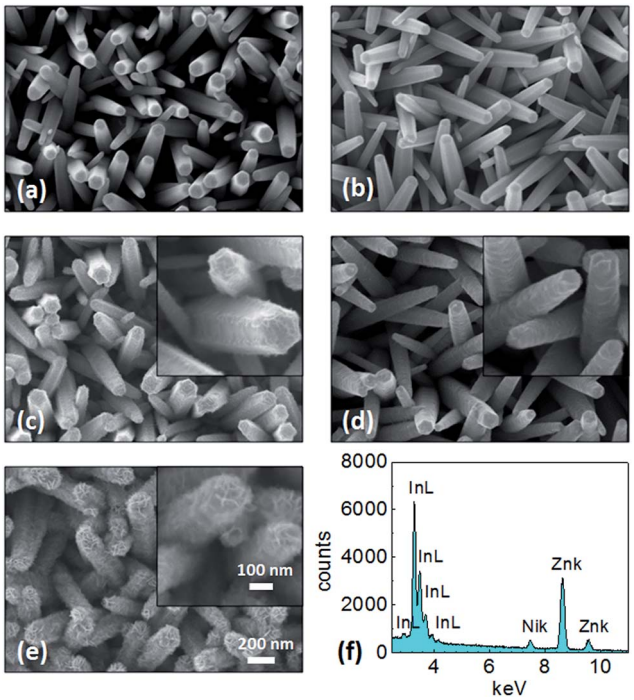

Fig. 1 SEM images of (a) ZnO NRs grown with 25 mM HMTA solution, (b) ZnO NRs grown with 50 mM HMTA solution, (c) sample 25-20, (d) sample 50-20, (e) sample 50-60. The scale bars in (e) are valid for all the images. The insets are higher magnification SEM images. (f) Portion of the EDX spectrum taken in the sample 50-60 (the whole spectrum is reported in Fig. S1†).

Table 1 Summary of the morphological features (average height, *h*, and lateral size, *d*) for the as-grown ZnO NRs synthesized with different HMTA concentrations and corresponding number of pulsed electrodeposition cycles used for the synthesis of $Ni(OH)_2$

Sample	[HMTA]	*h* [nm]	*d* [nm]	No deposition cycles of $Ni(OH)_2$
25-20	25 mM	650 ± 20	100 ± 30	20
50-20	50 mM	1000 ± 20	70 ± 20	20
50-40	50 mM	1000 ± 20	70 ± 20	40
50-60	50 mM	1000 ± 20	70 ± 20	60

electrodeposition, as summarized in Table 1. SEM micrographs of selected electrodes are shown in Fig. 1(c)–(e). The samples 25-20 and 50-20, Fig. 1(c) and (d), were prepared using 25 mM and 50 mM HMTA, respectively, during the ZnO growth and 20 electrodeposition cycles for $Ni(OH)_2$. The original array-shaped structured is maintained (see Fig. 1(a) and (b)) and $Ni(OH)_2$ nanoflakes look to be spread on the surface of the ZnO assuming different morphology due to the different surface area provided by the nanorods. The sample 25-20 is characterized by a ruffled morphology consisting of overlapping thin $Ni(OH)_2$ sheets, while the 50-20 shows a smoother feature. By increasing the number of electrodeposition cycles up to 60, a considerable surface roughness is attained with $Ni(OH)_2$ sheets aggregated in a porous shell, as shown in Fig. 1(e) for the sample 50-60 and Fig. S2† for 50-40. In addition, it is worth reporting that TEM analysis performed on electrochemically deposited $Ni(OH)_2$ nanoflakes on ZnO nanorods revealed that the $Ni(OH)_2$ shell is solidly attached to the surface of ZnO.[18] The EDX analysis was performed in order to check the elemental composition of the electrodes. The spectrum of the sample 50-60 is depicted in Fig. 1(f), revealing the signal related to nickel in addition to the expected strong peaks for indium (from the substrate) and zinc.

To evaluate the electrochemical properties of the final $Ni(OH)_2$/ZnO electrodes, cyclic voltammetry (CV) was employed over a potential range from 0 V to 0.8 V in 0.1 M NaOH solution. Fig. 2 shows the CVs of the samples 25-20, 50-20, 50-60 acquired at scan rate of 50 mV s^{-1} (*vs.* SCE). The anodic and cathodic peaks, clearly visible in all the curves, are attributed to reversible transition Ni^{2+}/Ni^{3+} in alkaline medium, according to the following redox reaction:[8,24]

$$Ni(OH)_2 + OH^- \leftrightarrow NiOOH + H_2O + e^- \quad (3)$$

It is worth reporting that all the samples showed stable voltammograms after few (5–6) cycles, indicating that the surface area of $Ni(OH)_2$ nanoflakes is almost immediately electrochemically activated. The cyclic voltammograms of bare ITO and ZnO NRs/ITO samples are reported in Fig. S3,† showing no electrochemical features. The CVs of the samples 25-20 and 50-20 present comparable enclosed area and slightly different intensity and position of the peak current. Increasing the amount of electrodeposited $Ni(OH)_2$, *via* setting the deposition cycle number at 60, lead to a voltammogram with higher peak current and wider enclosed area (see blue curve in Fig. 2) that

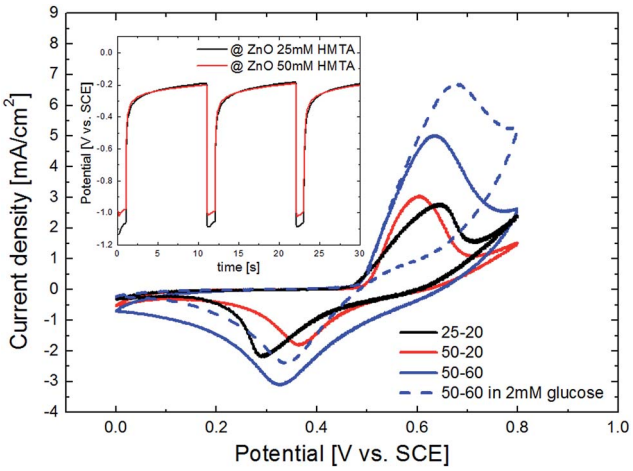

Fig. 2 Cyclic voltammograms of 25-20, 50-20, 50-60 in 0.1 M NaOH solution (scan rate 50 mV s^{-1}). The dashed line refers to the CV of 50-60 in 0.1 M NaOH solution containing 2 mM of glucose. The inset shows the CP curves related to the first 3 cycles of pulsed electrodeposition of $Ni(OH)_2$ on ZnO NRs grown at 25 and 50 mM HMTA.

indicate a larger active surface area for the formation of NiOOH species.[16] Moreover, the samples 50-20 and 50-60, having ZnO NRs grown at 50 HMTA as underlying layer, exhibit a very similar trend that differs from the CV shape recorded for the sample 25-20 (especially in terms of anodic–cathodic peak potential spacing). The inset in Fig. 2 reveals the chronopotentiometry (CP) curves acquired during the pulsed electrodeposition of $Ni(OH)_2$ on ZnO NRs synthesized with 25 mM and 50 mM HMTA, respectively. The potential peak, reached during the current-on time, is higher in the 25-20 sample which presumably offer an electrical path with higher resistance than the 50-20 sample, whose surface area is well larger (see *d* and *h* values in Table 1). This points out that the 50 HMTA samples shows some advantages in terms of electrical transport feature.

Taking into account all these findings, it is therefore reasonable to assume that different synthetic conditions of the ZnO NRs and their resulting morphological properties affect the catalytic action of $Ni(OH)_2$ nanoflakes deposited on them. To prove the catalytic activity of $Ni(OH)_2$ nanoflakes for the oxidation of the glucose, cyclic voltammetry tests were performed with 2 mM glucose in 0.1 M NaOH. Fig. 2 reports, in particular, the CV for the sample 50-60 (dashed line) showing the increase of anodic peak current due to the oxidation of glucose catalyzed by Ni^{3+} species:[5]

$$NiOOH + glucose \rightarrow Ni(OH)_2 + glucolactone \quad (4)$$

Simultaneously, a decrease of the cathodic current peak is observed, attributable to the increased concentration of Ni^{2+} during the process.[17] Similar CV have been observed for other samples. Fig. 3(a) shows the CVs acquired at different scan rates (10–150 mV s^{-1}) in 0.1 M NaOH containing 1 mM glucose, revealing that the anodic and cathodic peaks symmetrically vary without significant changing in the shape of the curves. Moreover, the absolute values of both the reduction and the oxidation peak currents increase with the scan rate and a linear

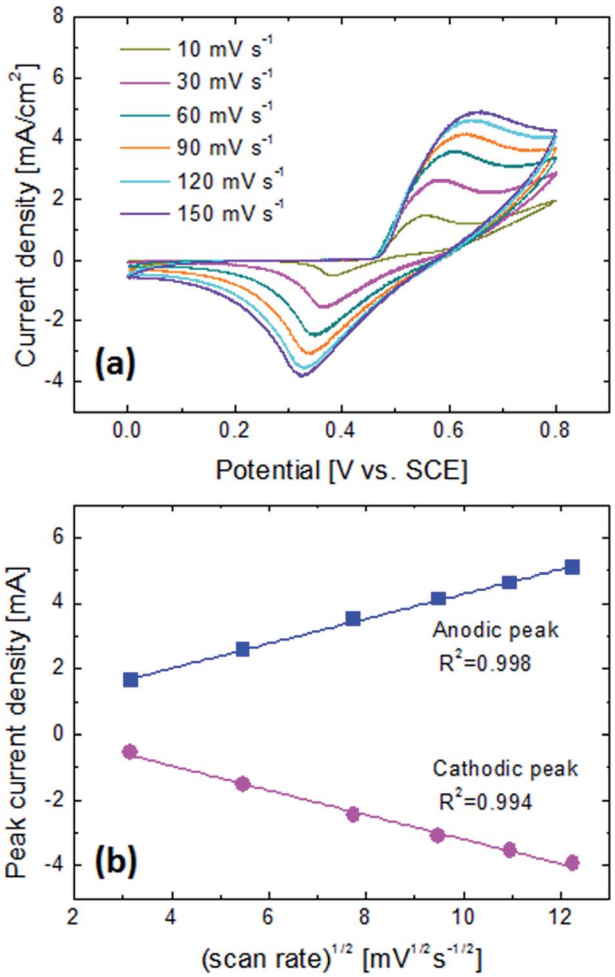

Fig. 3 (a) CV curves of 50-20 in 0.1 M NaOH solution containing 1 mM of glucose at different scan rate. (b) Experimental variation of anodic and cathodic peaks with (scan rate)$^{1/2}$ and corresponding linear fit line (the coefficients of determination, R^2, are also reported).

relationship was found with the square root of scan rates, as indicated in Fig. 3(b). This suggests that the electrochemical reaction is a diffusion-limited process.[9,16,25]

The amperometric responses of the samples upon successive addition of certain amount glucose to the electrolyte were carried out. The measurements were performed under continuous stirring in order to promptly homogenize the glucose in the solution. The value of the applied potential has been widely proven to affect the chronoamperometric response of glucose sensor electrodes.[8,11,13] Therefore, an appropriate choice of the working potential is important to properly compare the sensitivity of different samples. Since the potential at which the Ni^{2+}/Ni^{3+} occurs is slightly different for the samples (Fig. 2), it was necessary to run chronoamperometry at different potentials. Moreover, in order to avoid too high background currents, the working potentials were fixed lower than those of corresponding anodic peaks (10% lower than the peak current densities). Fig. 4 reports the current density *vs.* time for 25-20 and 50-20, carried out at 0.60 and 0.55 V respectively. The measurement was carried out by injecting specific amount of glucose solution

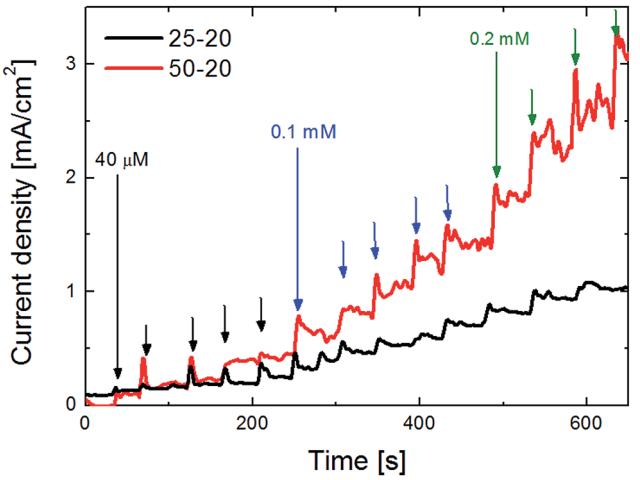

Fig. 4 Current density–time response of the sample 25-20 and 50-20 for successive addition of glucose in 0.1 M NaOH.

into the 0.1 M NaOH buffer every 40–50 s in such a way to increase the glucose concentration of the buffer by definite amounts (40 μM, 0.1 mM or 0.2 mM), as indicating by the arrows. The responses show a step-like behavior following the gradual addition of glucose. The noise signal becomes higher as the glucose concentration increases, especially for the sample 50-20, because of the accumulation of reaction intermediates on the surface of the electrode.[4,10] The response time is less than 1 s for both electrodes indicating a quick response with a good electron transfer through $Ni(OH)_2$/ZnO/ITO electrodes.

The linear ranges of the calibration curves, reported in Fig. 5, result from the chronoamperometric analyses considering the average current density values measured between successive glucose injection.[11,14] The lower sensitivity is achieved for the sample 25-20 (0.60 mA mM^{-1} cm^{-2}) while the highest (1.85 mA mM^{-1} cm^{-2}) is for the sample 50-20. Taking into account that these samples were subjected to the same number of electrodeposition cycles, with fixed current density, it can be argued that the underlying ZnO NRs array plays a key role in

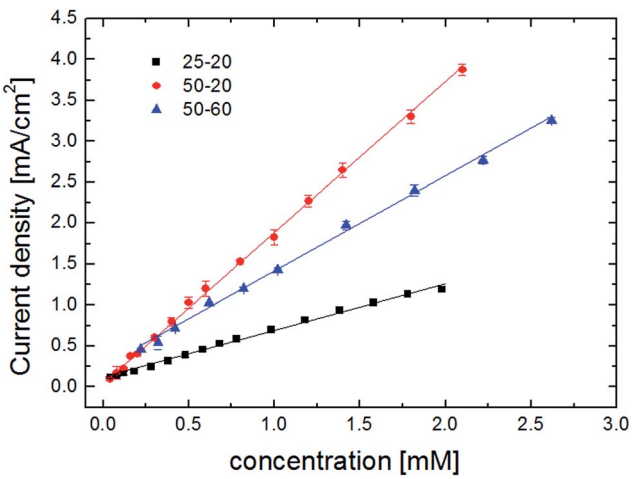

Fig. 5 Calibration curves of samples 25-20, 50-20, 50-60 for several addition of glucose in 0.1 M NaOH solution.

determining the sensing performance of the hierarchical structure. In particular, the shape and the distribution of the $Ni(OH)_2$ nanoflakes deposited on ZnO depend on the different sizes of the NRs, coming just from the variation of HMTA concentration during their synthesis. This causes changes in the electrochemical behavior (as above discussed in Fig. 2) and in the glucose detection process. The graph in Fig. 5 reports also the calibration curve for the sample 50-60 revealing an unexpected lower sensitivity (1.42 mA mM^{-1} cm^{-2}) compared to 50-20 sample.

In general, it is observed that the better the electrochemical feature is, the more efficient the amperometric sensing performance results.[8,16] In this case, the higher number of deposition cycles (with consequent increase of the amount of deposited $Ni(OH)_2$) leads to the formation of a surface morphology that, although it retains the nanoflakes form with high exposed area, may slow down the electrode kinetics, in terms of easy diffusion and migration of glucose and its oxidation products. Therefore, even though 60 cycles improve the ZnO NR coverage, this represents a drawback for sensing purposes. Not always the most porous architecture gives the best result and, in addition, the high background current is a detrimental factor for glucose sensing performance.[11] Table 2 lists the values of the sensitivity and the linear range of the samples, including the performance of the sample 50-40 (see Fig. S4†), synthesized with 50 mM HMTA for ZnO NRs and 40 deposition cycles, that confirms the trend of decreasing sensitivity as the number of electrodeposition pulses increases.

Recently, Yang *et al.*[16] reported on the sensing performance of $Ni(OH)_2$ hollow nanorod deposited by CBD using electrodeposited ZnO NRs as template. They achieved a maximum sensitivity of about 0.35 mA mM^{-1} cm^{-2} (value extracted from ESI†[16]) when the ZnO NR are present, while the sensitivity significantly increases (1.57 mA mM^{-1} cm^{-2}) if the NRs were removed, as due to a larger surface area provided by the hollow structure. Our best result (1.85 mA mM^{-1} cm^{-2}) reported here can thus be further improved if NRs were removed also in our case. Still, here we are interested to find the best synthetic procedure of ZnO NRs as template (not to be removed) for $Ni(OH)_2$ nanoflakes. The specificity is an important issue for biological sensing. Uric acid (UA), ascorbic acid (AA) and acetaminophen (AC) are common electroactive species that can interfere with the detection of glucose in physiological solution.[9–11] Fig. 6(a) reports the interference test of the sample 25-20 carried out by evaluating the amperometric response to consecutive additions of glucose (0.2 mM), UA (0.02 mM), AA (0.01 mM) and AC (0.01 mM), at 0.60 V. The concentration ratio

Table 2 Sensing parameters of samples 25-20, 50-20, 50-40 and 50-60

Sample	Sensitivity [mA mM^{-1} cm^{-2}]	Linear range [mM]
25-20	0.6	0.04–1.98
50-20	1.85	0.04–2.10
50-40	1.42	0.04–1.30
50-60	1.16	0.20–2.60

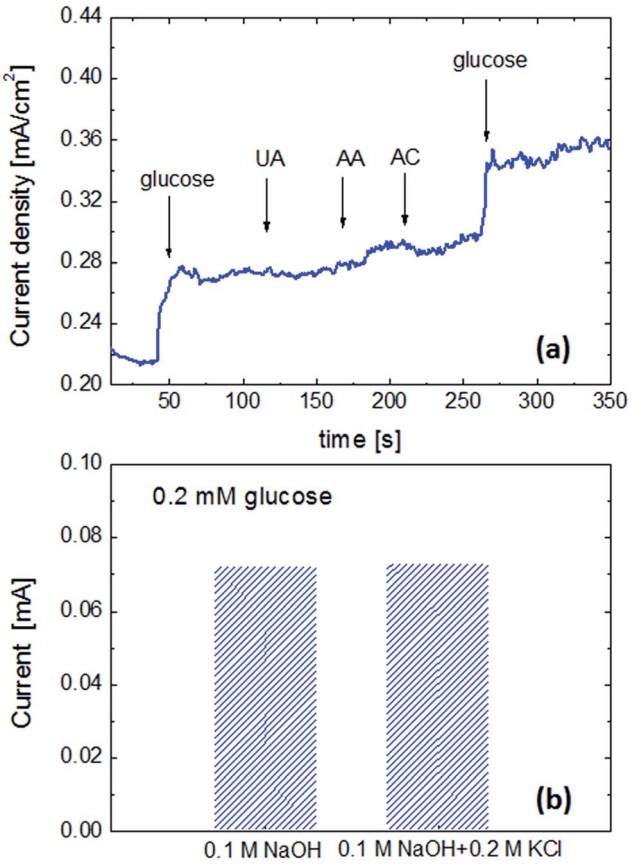

Fig. 6 (a) Interference test showing the current increase after the addition of 0.2 mM glucose, 0.02 mM UA, 0.01 mM AA and 0.01 mM AC; (b) test indicating the current response to the addition of 0.2 mM glucose with and without the presence of 0.2 M KCl.

between the interfering species and glucose mimics the physiological levels. Only the first and second additions of glucose provide a remarkable change in the current revealing a good selectivity for glucose sensing. Moreover, it is worth highlighting the stability of the current value over the time, after the glucose injections. A further confirmation of the sensing specificity was provided by the cyclic voltammetry carried out in 0.1 mM NaOH solution with subsequent addition of glucose, AC, AA, UA and glucose. The resulting CVs are presented in Fig. S5† and show they show an increase of the peak current only in correspondence of the additions of glucose. The good selectivity can be due to the electrostatic repulsion between $Ni(OH)_2$ and the interfering species at pH 13 that prevents the electrochemical oxidation at the electrode surface.[7,16] The stability of the electrodes were also investigated in presence of chlorine ions that has been shown to limit the sensitivity of different non-enzymatic sensor electrode.[4,11] Fig. 6(b) shows that there is no variation in the current gain due to the addition of 0.2 mM glucose in presence of 0.2 M KCl. Similar results were obtained for all the sample studied in this work.

The long-term stability was evaluated by measuring the current response to glucose addition of the samples (stored at room temperature) at regular time intervals for 40 days. No significant change (5% loss in average) was observed,

demonstrating a satisfactory stability of the electrodes. A comparison between some low-cost non-enzymatic glucose sensors based on Ni nanostructures is reported in Table S1.† The electrodes proposed in this work show the higher sensitivity and, moreover, they are tested to work also in case of chloride poisoning.

Conclusions

In conclusion, we reported on the low-cost, fully-chemical synthesis of hierarchical nanostructures consisting of $Ni(OH)_2$ nanoflakes electrodeposited on CBD grown ZnO NRs. The effects of the chemical (HMTA concentration) and electrochemical (deposition cycles) synthetic parameters on the morphology were examined and an appropriate adjusting of the experimental design was proven to improve the glucose detection performance of the final electrodes. The higher glucose sensitivity (1.85 mA cm^{-2} mM^{-1}) was reached for ZnO NRs with average lateral size of 70 and a height of 1000 nm covered by $Ni(OH)_2$ nanoflakes through 20 cycles of pulsed electrodeposition. The electrodes showed high detection selectivity (in presence of UA, AA and AC), long-term stability and unchanged performance in chloride poisoning condition. The reported preparation method and the results related to the glucose sensing show that $Ni(OH)_2$/ZnO hierarchical nanostructure represent a promising approach for low-cost glucose sensors.

Acknowledgements

The authors wish to thank K. Iwu and E. G. Barbagiovanni (CNR-IMM MATIS) for fruitful scientific discussion and G. Pantè (CNR-IMM MATIS) for technical assistance.

References

1 Z. Ren, Y. Guo, C. Liu and P. Gao, *Front. Chem.*, 2013, **1**, 1–22.
2 K. E. Toghill, L. Xiao, M. A. Phillips and R. G. Compton, *Sens. Actuators, B*, 2010, **147**, 642–652.
3 J. Wang, L. Chen and K. Ho, *ACS Appl. Mater. Interfaces*, 2013, **5**, 7852–7861.
4 K. Tian, M. Prestgard and A. Tiwari, *Mater. Sci. Eng., C*, 2014, **41**, 100–118.
5 C. Zhao, C. Shao, M. Li and K. Jiao, *Talanta*, 2007, **71**, 1769–1773.
6 S. Lin, S. Chang and T. Hsueh, *Appl. Phys. Lett.*, 2014, **104**, 193704.
7 X. Niu, X. Li, J. Pan, Y. He, F. Qiu and Y. Yan, *RSC Adv.*, 2016, **6**, 84893.
8 Y. Zhang, F. Xu, Y. Sun, Y. Shi, Z. Wen and Z. Li, *J. Mater. Chem.*, 2011, **21**, 16949.
9 P. Yang, X. Tong, G. Wang, Z. Gao, X. Guo and Y. Qin, *ACS Appl. Mater. Interfaces*, 2015, **7**, 4772–4777.
10 G. Wang, X. Lu, T. Zhai, Y. Ling, H. Wang, Y. Tong and Y. Li, *Nanoscale*, 2012, **4**, 3123.
11 K. Iwu, A. Lombardo, R. Sanz, S. Scirè and S. Mirabella, *Sens. Actuators, B*, 2016, **224**, 764–771.
12 W. Lu, X. Qin, A. Asiri, A. Al-Youbi and X. Sun, *Analyst*, 2013, **138**, 429–433.
13 X. Li, J. Yao, F. Liu, H. He, M. Zhou, N. Mao, P. Xiao and Y. Zhang, *Sens. Actuators, B*, 2013, **181**, 501–508.
14 A. Safavi, N. Maleki and E. Farjami, *Biosens. Bioelectron.*, 2009, **24**, 1655–1660.
15 P. Sivasakthi, G. Ramesh Bapu and M. Chandrasekaran, *Mater. Sci. Eng., C*, 2016, **58**, 782–789.
16 J. Yang, M. Cho and Y. Lee, *Sens. Actuators, B*, 2016, **222**, 674–681.
17 Z. Shen, W. Gao, P. Li, X. Wang, Q. Zheng, H. Wu, Y. Ma, W. Guan, S. Wu, Y. Yu, *et al.*, *Talanta*, 2016, **159**, 194–199.
18 I. Lo, J. Wang, K. Huang, J. Huang and W. Kang, *J. Power Sources*, 2016, **308**, 29–36.
19 V. Strano, R. Urso, M. Scuderi, K. Iwu, F. Simone, E. Ciliberto, C. Spinella and S. Mirabella, *J. Phys. Chem. C*, 2014, **118**, 28189–28195.
20 V. Strano, E. Smecca, V. Depauw, C. Trompoukis, A. Alberti, R. Reitano, I. Crupi, I. Gordon and S. Mirabella, *Appl. Phys. Lett.*, 2015, **106**, 013901.
21 S. Tong, Y. Xu, Z. Zhang and W. Song, *J. Phys. Chem. C*, 2010, **114**, 20925–20931.
22 L. Vayssieres, *Adv. Mater.*, 2003, **15**, 464–466.
23 L. Greene, M. Law, J. Goldberger, F. Kim, J. Johnson, Y. Zhang, R. Saykally and P. Yang, *Angew. Chem., Int. Ed.*, 2003, **42**, 3031–3034.
24 G. Fu, Z. Hu, L. Xie, X. Jin, Y. Xie, Y. Wang, Z. Zhang, Y. Yang and H. Wu, *Int. J. Electrochem. Sci.*, 2009, **4**, 1052–1062.
25 A. J. Bard and L. R. Faulkner, *Electrochemical Methods: Fundamental and Applications*, Wiley, New York, 2nd edn, 2001, ch. 6, pp. 228–232.